Research Article

Rockburst Characteristics and Mechanisms during Steeply Inclined Thin Veins Mining: A Case Study in Zhazixi Antimony Mine, China

Yuanjun Ma,[1,2] Changwu Liu [iD],[1] Fan Wu,[3] and Xiaolong Li[1]

[1]*State Key Laboratory of Hydraulic and Mountain River Engineering, College of Water Resource and Hydropower, Sichuan University, Chengdu 610065, China*
[2]*China Gezhouba Group Explosive Co., Ltd., Chongqing 401121, China*
[3]*Institute of Disaster Management and Reconstruction, Sichuan University-The Hong Kong Polytechnic University, No. 1 Huanghe Road, Chengdu 610065, China*

Correspondence should be addressed to Changwu Liu; liuchangwu@scu.edu.cn

With the increase of mining depth, rockbursts have become important safety problems in Zhazixi Antimony Mine, where overlying strata exceed 560 m. Due to the small spacing between the steeply inclined veins, mining activities have great influences on rockbursts of adjacent veins. In order to study rockburst characteristics and mechanisms in Zhazixi Antimony Mine, in situ measurement, field geological survey, uniaxial compression tests, and numerical simulation are conducted to analyze rockburst proneness and simulate the elastic strain energy accumulation characteristics. Consequently, rockburst proneness criteria are established on the basis of experimental results to propose the necessary lithologic conditions for rockburst aiming to Zhazixi Antimony Mine. Rockburst dangerous districts are defined based on high stress concentration and elastic strain energy distribution characteristics in mining process obtained by theory analysis and numerical simulation. Accordingly, it is suggested that thrown-type rockbursts mainly occur in massive stibnite of ventilation shafts and stopes where the elastic strain energy exceeds $300 \, \mathrm{kJ \cdot m^{-3}}$, spalling-type rockbursts generally appear in slate of roadways where the elastic strain energy exceeds $100 \, \mathrm{kJ \cdot m^{-3}}$, and ejection-type rockbursts arise in different rock masses under a certain condition. Last but not the least, prediction results are basically consistent with statistics data of rockburst events after comparative analysis.

1. Introduction

A rockburst is a sudden dynamic instability phenomenon under excavation unloading conditions of high geostress areas [1]. As excavation depth increases progressively, rockburst accidents occur frequently, which can lead to schedule delays, equipment damage and even life-threatening situations. In recent years, different kinds of projects have suffered from rockbursts, e.g., hydropower projects [2, 3], tunnels [4, 5] and mines [6–8], resulting in huge direct and indirect economic losses. It is obviously beneficial and significant to acquaint its mechanism in order to control rockbursts with proper measures.

Actually, many methods, such as case analysis [9], in situ stress measurement [10, 11], rock mechanics tests [12, 13], microseismic monitoring [2, 14], numerical simulation [15–17], etc., have been applied to study rockburst mechanisms in different projects. Although there is no consensus on the mechanism of rockbursts due to complexity and hidden nature of the subsurface geological conditions, some achievements of previous researches have thoughtful and profound effects. Driad-Lebeau [18] proposed that structurally complete rock combined with high horizontal tectonic stresses was responsible for rockbursts. Zhou et al. [19] demonstrated that preexisting cracks of rock masses were beneficial to abrupt energy release stored in rock masses,

coming into being rockbursts under certain conditions. Holub and Petros [20] discussed the thick and integrity strata were contributed to mining-induced seismicity, which was one of the characteristics of rockburst. Lu et al. and Meng et al. [21, 22] indicated geological structures, such as faults and joints, brought about stress increase sharply, which easily lead to rockbursts. Yang et al. [4] presented high in situ stresses were the main factor that caused strain energy accumulation and gave rise to rockbursts in the strong rock. Zhu et al. [16] emphasized great importance should be attached to rockbursts bought by dynamic disturbance during underground mining.

However, most of the research studies focus on a single roadway or stope, not much attention have been dedicated to the interaction of adjacent work faces. In particular, stresses redistribution is extremely complex influenced by adjacent working faces during steeply inclined veins mining. It should be noted that rockburst mechanisms have not yet been illuminated in steeply inclined mine. Besides, some measurements preventing or reducing rockburst disasters have been discovered unreasonable in application. Hence in this study, the characteristics of rockburst are first analyzed, and rockburst mechanisms are then comprehensively studied through rock mechanics experiment, theoretical research, and numerical simulation in Zhazixi Antimony Mine in China.

2. Engineering Background and Rockburst Characteristics

2.1. Engineering Background. Zhazixi Antimony Mine is located in the central of the Xuefeng arc structural belt, which is an essential Au-Sb-W metallogenic tectonic belt in Hunan province, China. It is hosted by the regional NE-trending Majiaxi fractures (F_3), which plays an important role in regional ore conduction. The deposit has more than 70 ore veins, and two-thirds of them have industrial exploitation value. The ore veins show inverted broom shape while the geological characteristics are as follows: thin thickness (0.02 m–10.29 m), long extent in strike (300–1000 m), steep dip (60°–90°). Furthermore, the ore veins are getting closer as the depth increases (Figure 1). According to the distance from F_3 fault, the thin ore veins are divided into three groups, i.e., no. 1–no. 20 ore veins belong to group I, no. 21–no. 33 ore veins belong to group II, and no. 34–no. 44 ore veins belong to group III.

2.2. Rockburst Characteristics. Considering the special geological conditions of ore veins, the shallow-hole shrinkage stoping method has been used in Zhazixi Antimony Mine since 1906. In order to raise economic efficiency, the high-grade ore veins such as no. 9 ore vein and no. 19 ore vein were preferred to be mined, while the poor ores were ignored. In recent years, the latent dangers in the mining area are gradually exposed with the deepening of mining. Rockbursts occurred first in a transport roadway when the opening depth reached 560 m (−115 m level). Especially, rockbursts are becoming increasingly frequent as mining
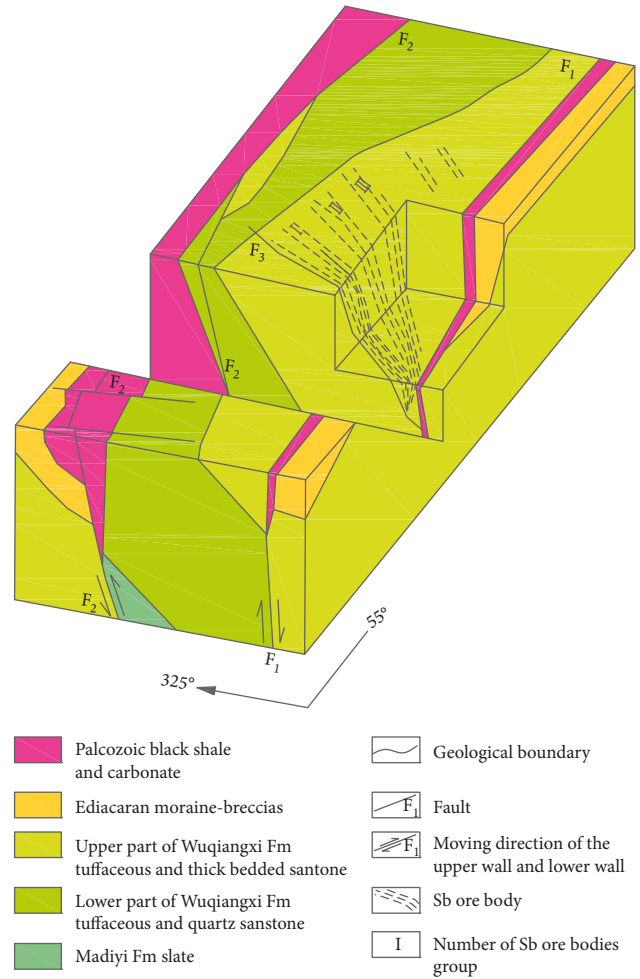

Figure 1: Fault block structure stereogram of Zhazixi Antimony Mine.

goes deeper. According to statistics data, there were more than 30 accidents of rockburst between May 2012 and May 2013. At present, the maximum mining depth has been extended to the depth of 650 m (−205 m level).

Rockburst mainly occurred in the transport roadway when mining depth was −115 m level where the surrounding rocks were relatively intact sandstone and slate with many endogenetic cracks (Figure 2). The initial stress equilibrium state of surrounding rock was disturbed after excavation. The tangential stress increased sharply, and the radial stress decreased, and tensile cracks extension was accelerated on the surface of roadway, resulting in multilayer lamellar spalling at the spandrel (Figure 3(a)). The thickness of spalling was less than 2 cm. Moreover, fresh rock surface was covered with white rock powder, which indicated the elastic strain energy stored in rock masses was released to crush internal rock masses without great influences on the projects. The fracture planes were characterized by honeycomb cracks.

However, when mining depth exceeded −160 m level, rockburst mainly occurred in the ventilation shaft or stope where the surrounding rocks were stibnite. As excavation gone into high go-stress areas, the elastic strain energy stored
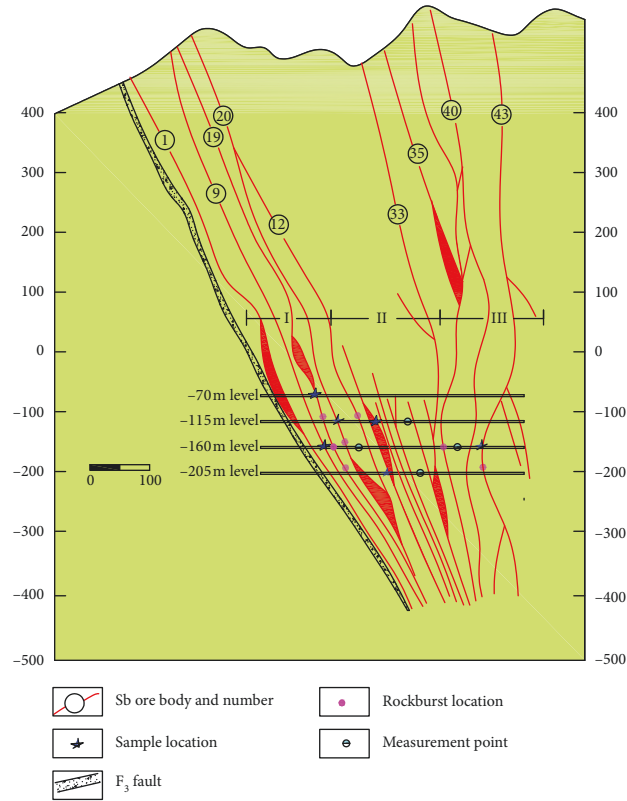
Figure 2: No. 0 exploratory grid cross section of Zhazixi Antimony Mine.

in rock masses progressively increased. Once confining pressure exceeded compressive strength of rock masses, the rock masses failure mode changed into fragile failure from plastic failure accompanied with an instantaneous impact failure. As a result, a large amount of rock masses were ejected or thrown out due to elastic strain energy release (Figure 3(b)), bringing great damages to projects. The fracture surface was similar to a dome.

Based on previous research results, many factors are considered to cause rockburst: high geostress, excavating-induced stresses, the dynamic disturbance of adjacent ore vein mining, etc. A comprehensive understanding of how different factors affect rockburst is essential for rockburst mechanism and prediction. Therefore, a systematic research has been carried out as shown in Figure 4.

3. Experimental Studies

3.1. In Situ Stress Measurements

3.1.1. The Measurement Method.
At present, stress relief method by overcoring is one of the in situ stress measuring methods with high applicability and reliability [23]. Its measuring tools include hollow inclusion strain gauge, geological drilling rig, and drill pipe of $\Phi 130$ mm and $\Phi 45$ mm. The drill holes with different diameters ($\Phi 130$ mm and $\Phi 45$ mm) of measurement points separate the core from the surrounding rocks, which relief the three dimensional stress. In the process of stress relief, the core has a little elastic deformation. Therefore, the in situ stress could be calculated by the elastic theory after hollow inclusion strain gauge measures the strain elastic deformation value. However, it must be noted that the measurement points should be set in the in situ stress areas of intact rock mass undisturbed by excavation. Generally speaking, the depth of drilling holes should be 3–5 times the width of the roadway. The procedure of in situ stress measurement is shown in Figure 5.

The kx-81 hollow inclusion strain gauges were made by Chinese Academy of Geological Sciences (CAGS). It consists of three groups of resistance strain rosette, and each group is composed of four strain gauges with 45° distribution. A single hollow inclusion strain gauge can measure the three dimensional stress state of a borehole.

Considering the in situ stress has been measured in shallow part near the mine [24], four measurement points are layout at three levels in deep mining areas of Zhazixi Antimony Mine, i.e., −115 m level (burial depth 560 m), −160 m level (burial depth 605 m), and −205 m level (burial depth 650 m), respectively.

3.1.2. In Situ Stress Field Distribution

(1) Measurement Results. The kx-81 hollow inclusion strain gauge measured the strain value caused by stress relief (Figure 6), the stress relief curves of four points are shown in Figure 7, and the channel's sequence and orientation are shown in Figure 8. The stress relief curves have three stages with the increase of relief depth as follows: initial stage, strain data have no obvious changes at the beginning of the stress relief. Revulsion stage, strain data have strenuous changes
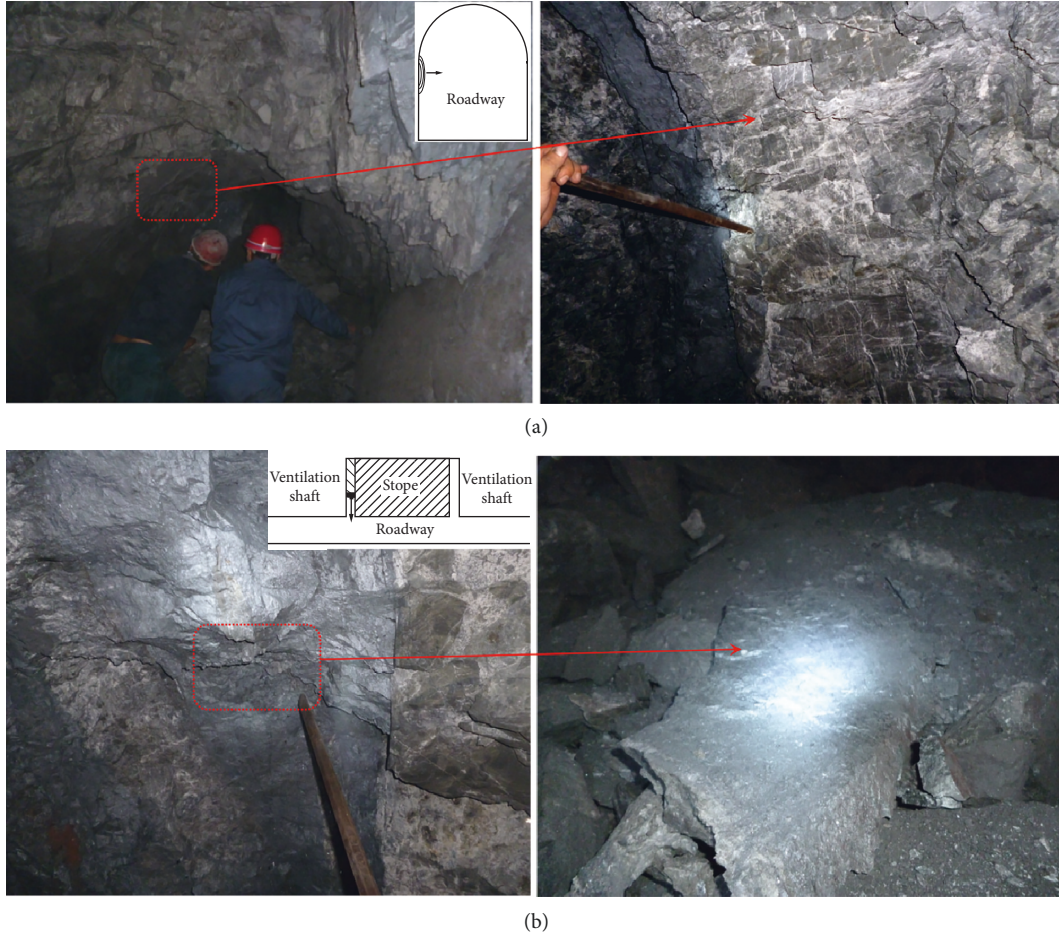
(a)

(b)

FIGURE 3: Typical rockbursts. (a) A spalling rockburst in a transport roadway at −115 m level. (b) A strong rockburst in a ventilation shaft at −160 m level.

with the increase of relief depth. Steady stage, strain data tend to be stable when the stress relief positions gradually remove from the top of strain gauge. The variation rule of most curves is reasonable, indicating that the strain gauge works normally, and the measured data are reliable.

The relationship between the stress tensor $[\sigma]$ and strain tensor $[\varepsilon]$ can be expressed as follows [9]:

$$[\varepsilon]^{12*1} = [A]^{12*6}[\sigma]^{6*1}, \tag{1}$$

where A is closely related to Poisson's ratio, Young's modulus, and coefficients k_1, k_2, k_3, and k_4 of rock masses at measurement points. All these parameters required for calculation are obtained from confining pressure calibration tests of borehole cores. A special math software developed by CAGS was used to calculate the values and directions of three principal stresses (Table 1).

(2) In Situ Stress Field. Based on the calculation results of four measurement points associated with the geological structure investigation in this area, in situ stress field distribution characteristics of Zhazixi Antimony Mine could be easily analyzed. First of all, the major principal stress (σ_H) is dominated by horizontal tectonic stress according to the angle between the major principal stress (σ_H) direction of

each measurement point, and the horizontal plane is less than 30°. In addition, the azimuth angles of major principal stress (σ_H) are 246°~261° with small amplitude of change, and the major principal stress (σ_H) direction of Zhazixi Antimony Mine in deep mining area is NEE-SWW. Furthermore, the principal stresses increase as the depth extends from level −75 m to level −205 m. Moreover, the major principal stress exceeds 20 MPa, which indicates that it belongs to the high stress zone. Combined with the shallow measurement results, the principal stress distribution regulations is as follows:

$$\left.\begin{array}{l} \sigma_H = 0.026h + 4.704 \\ \sigma_v = 0.014h + 4.006 \\ \sigma_h = 0.016h + 2.593 \end{array}\right\}, \tag{2}$$

where σ_H, σ_v, and σ_h represent the major principal stress, intermediate principal stress, and minor principal stress, respectively, and h is the depth.

3.2. Rockburst Proneness Analysis. There are many factors causing rockbursts because of the complexity of underground engineering. With respect to the influence of internal aspects, rock masses should be integral and have high
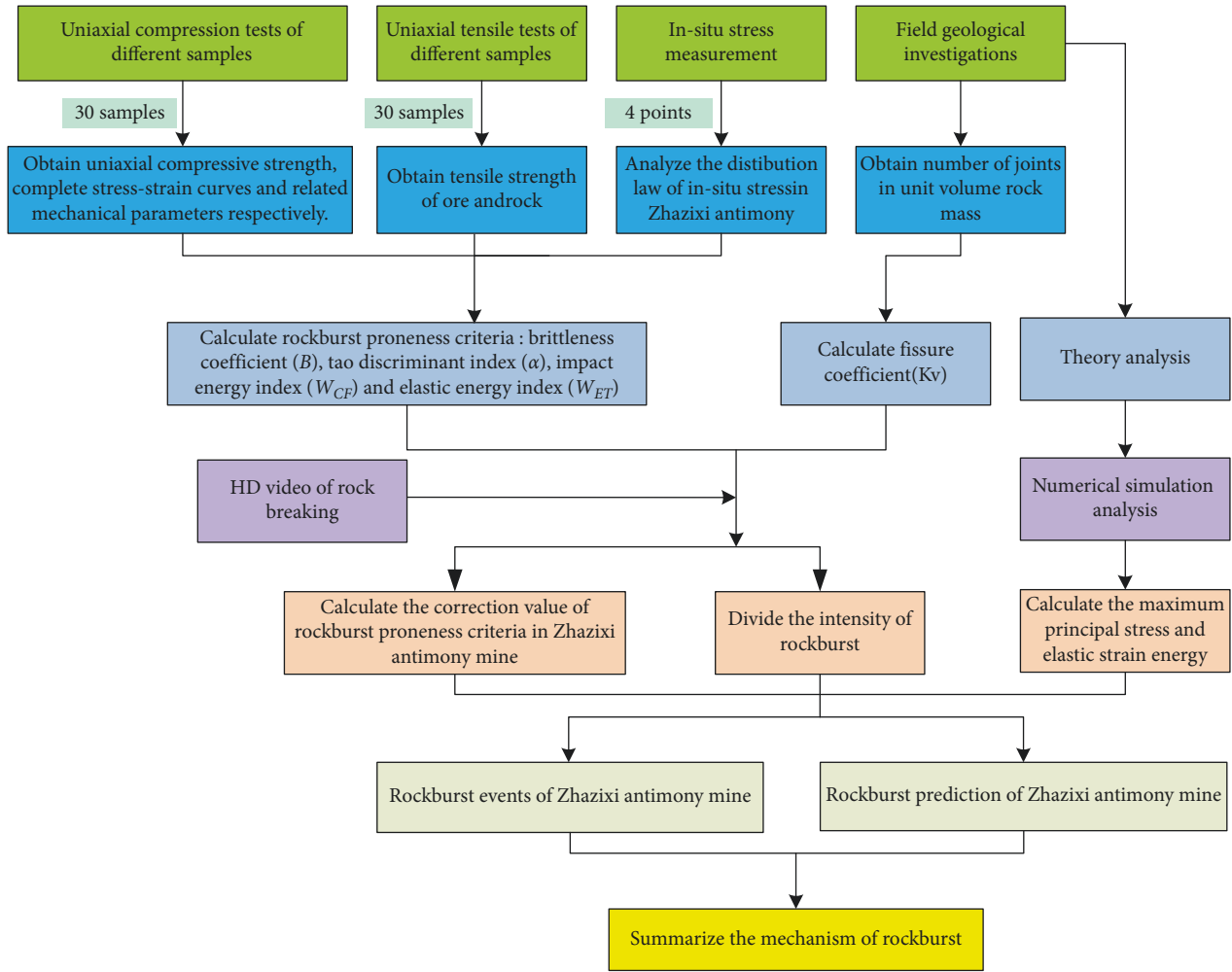
FIGURE 4: The block diagram of rockburst mechanism in Zhazixi Antimony Mine.

compression strength to have the ability of storing elastic strain energy. With respect to the influence of external factors, excavation areas should have high stresses which engender enough elastic strain energy. Rockbursts will occur only if the two aspects are satisfied at the same time.

Zhazixi Antimony Mine is mainly composed of six kinds of rocks: slate, tuffaceous slate, quartz sandstone, tuffaceous sandstone, massive stibnite, and disseminated stibnite. The uniaxial compression test is as shown in Figure 9. Rock mechanical properties under uniaxial compression are shown in Table 2.

Rockburst proneness is mainly used for qualitative analysis of rockburst. Many criteria and indexes have been proposed to define and forecast rockbursts. Combined with the field conditions of Zhazixi Antimony Mine, five evaluation indicators have been studied: fissure coefficient, brittleness coefficient, tao discriminant index, impact energy index, and elastic deformation energy index, respectively.

Fissure coefficient (K_v) reflects the overall stability of rock mass and capacity to store elastic strain energy, which has been obtained based on the number of structural plane in the unit volume of rock mass [25]. Brittleness coefficient (B) can be presented as the ratio of uniaxial compression strength (USC) to tensile strength (σ_t), which is calculated based on physical and mechanical experiments (Table 2). Tao discriminant index (a) considers the relationship between the major principal stress (σ_1) and USC. Impact energy index (W_{CF}) illustrates the intensity of energy released after the rocks failure under uniaxial compression loading, which can be displayed by the area ratio of prepeak strength and postpeak strength according to the complete stress-strain curves (Figure 10). Elastic energy index (W_{ET}) manifests the elastic energy stored in rocks before the peak strength, which is direct correlation with USC and Young's modulus.

Five rockburst proneness criteria [26] have been calculated on account of different test results (Table 3). Each index can be used to evaluate rockburst; however, a single index has large deviation due to complex geological structure and lithologic distribution. Five main indicators combined together can effectively improve the accuracy rate.

Consequently, rockbursts will occur only if all requirements of Equation (3) are met concurrently during deep mining in Zhazixi Antimony Mine. Its intensity can be appraised depending on other classifications.
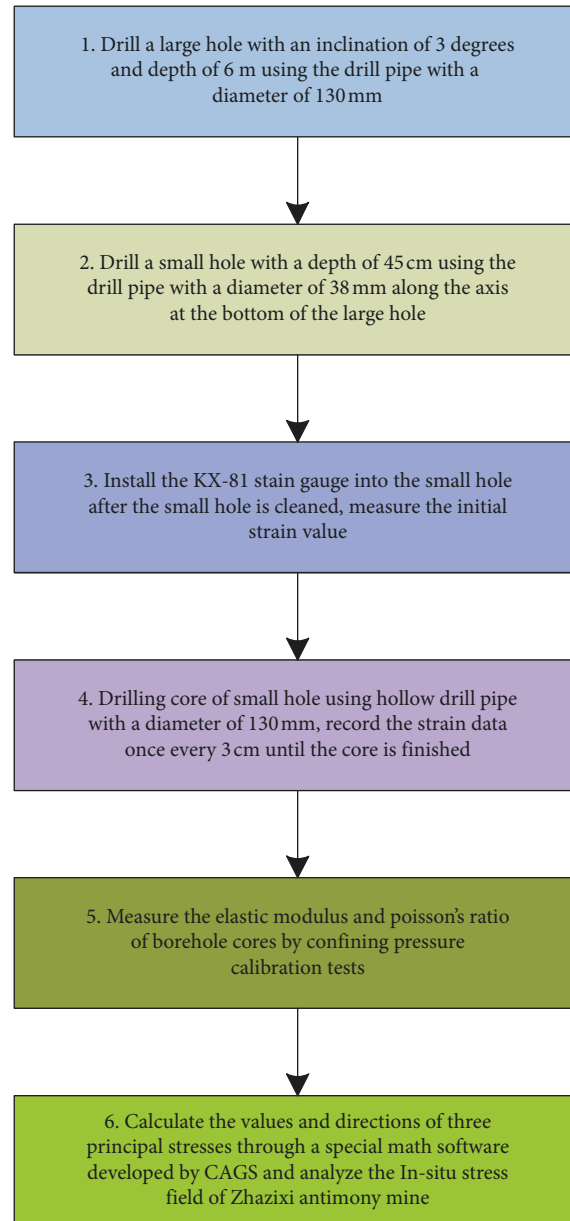
1. Drill a large hole with an inclination of 3 degrees and depth of 6 m using the drill pipe with a diameter of 130 mm

2. Drill a small hole with a depth of 45 cm using the drill pipe with a diameter of 38 mm along the axis at the bottom of the large hole

3. Install the KX-81 stain gauge into the small hole after the small hole is cleaned, measure the initial strain value

4. Drilling core of small hole using hollow drill pipe with a diameter of 130 mm, record the strain data once every 3 cm until the core is finished

5. Measure the elastic modulus and poisson's ratio of borehole cores by confining pressure calibration tests

6. Calculate the values and directions of three principal stresses through a special math software developed by CAGS and analyze the In-situ stress field of Zhazixi antimony mine

FIGURE 5: The block diagram of borehole stress relief method.
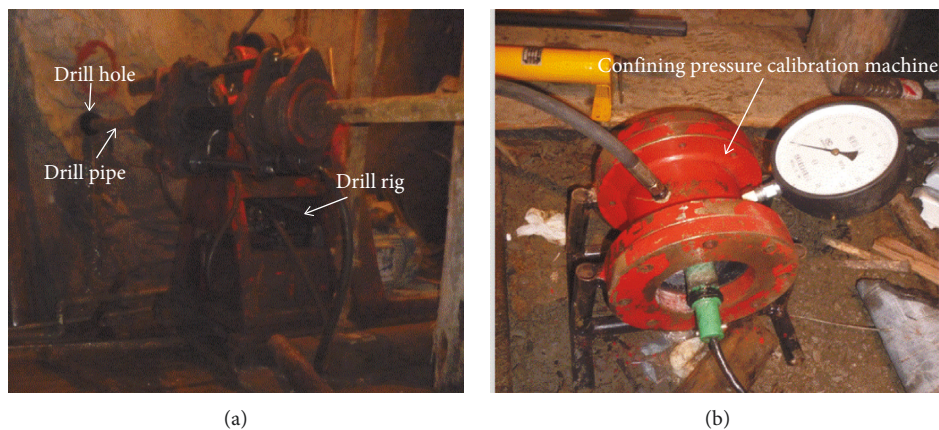

(a)

(b)

FIGURE 6: Stress relief tests. (a) Borehole overcoring. (b) Confining pressure calibration tests.
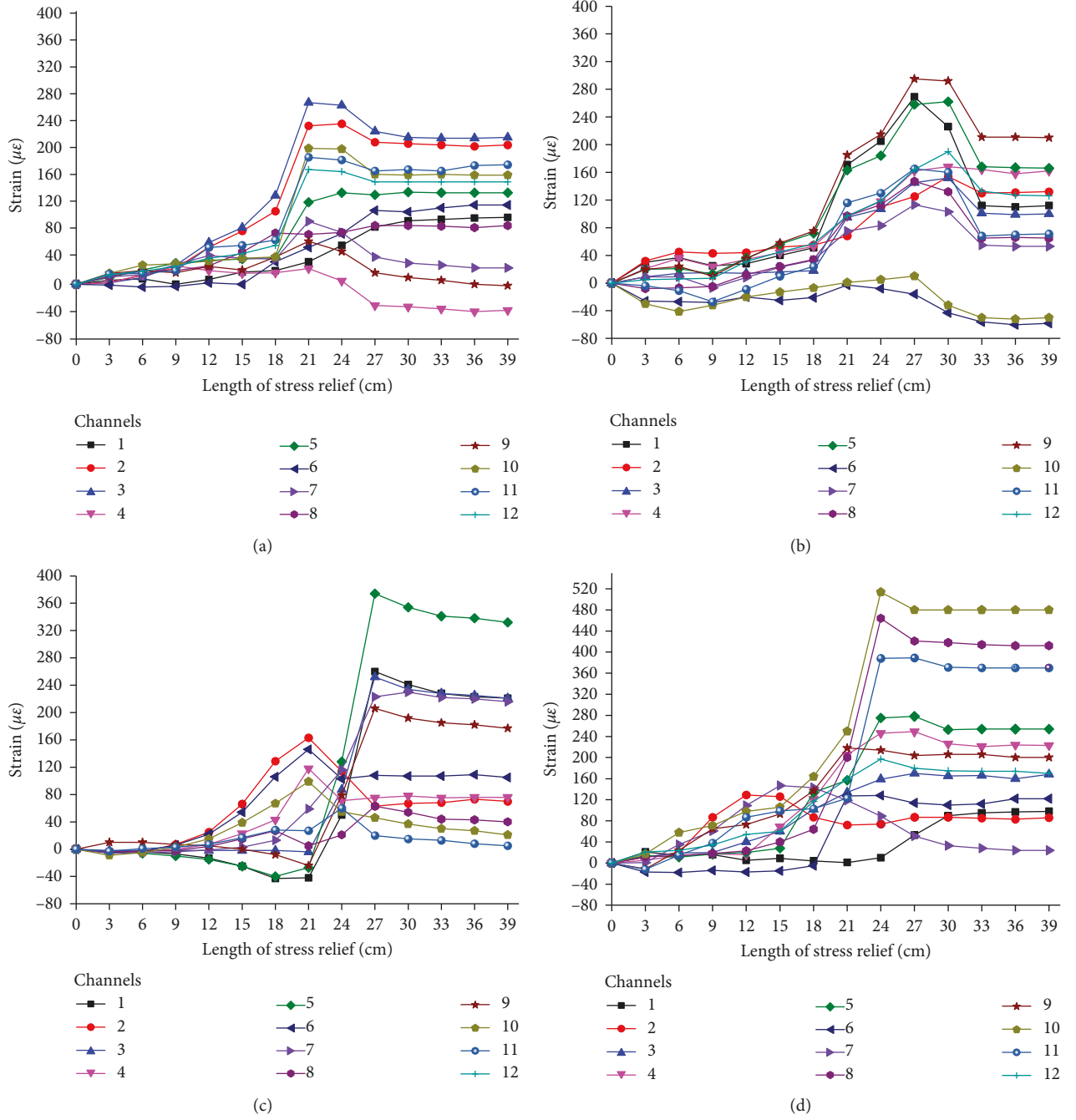
FIGURE 7: The stress relief curves. (a) Point 1. (b) Point 2. (c) Point 3. (d) Point 4.

$$
\left.\begin{array}{l}
K_v > 0.55 \\
B < 40 \\
\alpha < 11.4 \\
W_{CF} > 1 \\
W_{ET} > 100
\end{array}\right\}. \tag{3}
$$

From Equation (3), rockburst proneness criteria of Zhazixi Antimony Mine have been presented which reveal the internal requirement of rockburst in Zhazixi antimony. However, the external factors should be satisfied at the same time; that is, the rock mass must be in the high stress area, where the rock mass can store a larger elastic strain energy. As long as the internal factors and external factors are met, rockbursts can be accurately predicted in Zhazixi Antimony Mine.

4. Numerical Simulation Analysis

4.1. Theory Analysis. Rock masses keep stress equilibrium state before excavation, and they are affected by in situ stress (F_i). Once rock masses are excavated, stresses will be redistributed. In addition to the original stress, the
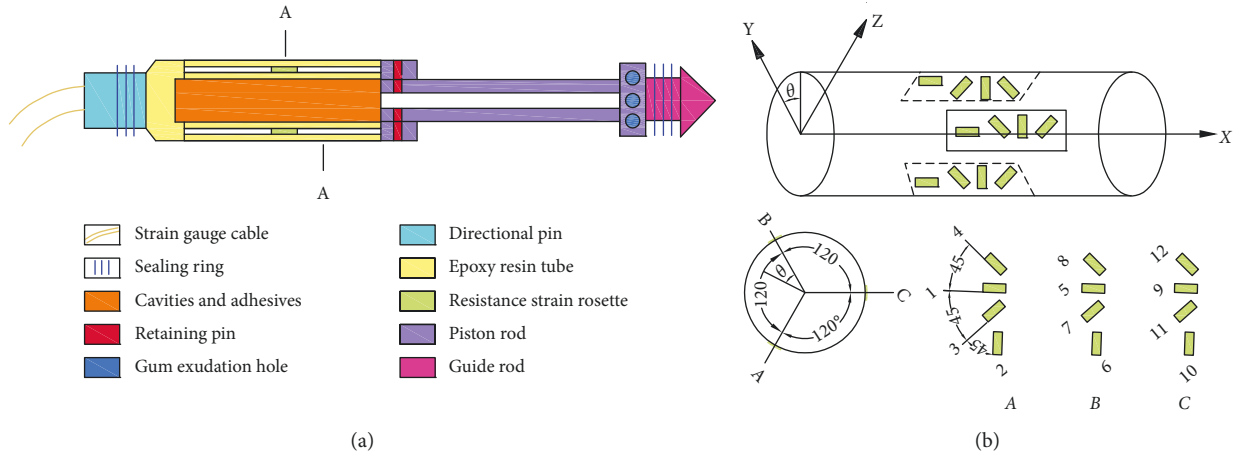
(a)

(b)

FIGURE 8: Hollow inclusion strain gauge.

TABLE 1: Measurement results of principal stress at four points of Zhazixi Antimony Mine.

No.	Level (m)	The major principal stress (σ_H)			The intermediate principal stress (σ_v)			The minor principal stress (σ_h)		
		Value (MPa)	Orientation (°)	Dip (°)	Value (MPa)	Orientation (°)	Dip (°)	Value (MPa)	Orientation (°)	Dip (°)
1	−115	16.36	257.31	3.25	8.00	346.49	165.94	7.36	180.03	104.44
2	−160	19.61	246.51	166.95	9.86	321.36	48.61	9.27	167.19	38.64
3	−160	18.76	260.83	165.27	12.79	306.92	69.24	10.43	174.67	14.30
4	−205	21.32	80.45	112.16	14.07	130.28	59.47	11.92	149.28	21.85
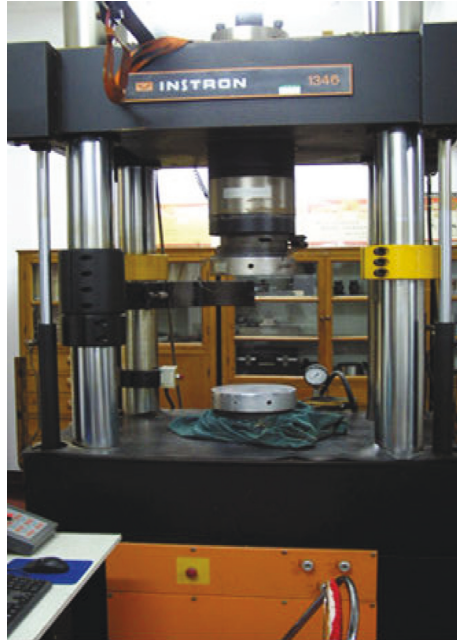
(a)
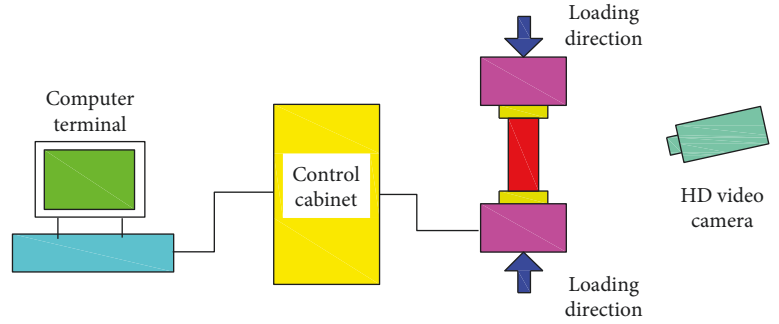
(b)

(c)

FIGURE 9: The experimental setup. (a) Universal hydraulic testing machine. (b) The experimental system. (c) Six kinds of rock samples.

surrounding rocks are affected by the disturbance stress of the mining (T_i), which keeps the rock masses being in static equilibrium under the action of specified body and surface forces (Figure 11).

After the rock masses are disturbed, the stored strain energy inside the rock can be embodied through the virtual work done by the body force F_i per unit volume and the surface force T_i per unit area [27]:

TABLE 2: Physical and mechanical properties of rocks.

Lithology	Density (g/cm³)	UCS (MPa)	Tensile strength (Mpa)	Poisson ratio	Cohesion (MPa)	Young's modulus (GPa)	Internal friction angle (°)
Slate	2.81	71.11	4.29	0.23	9	17.23	36.48
Tuffaceous slate	2.90	82.46	5.91	0.32	10.03	25.32	40.23
Quartz sandstone	2.75	65.17	7.45	0.20	17.32	23.65	45.32
Tuffaceous sandstone	2.70	76.12	6.06	0.26	11.21	35.95	41.94
Massive stibnite	3.84	114.34	4.57	0.21	11.84	58.23	49.80
Disseminated stibnite	3.12	93.15	5.54	0.25	9.86	43.12	50.61

$$W = \int_V F_i \delta u_i \, dv + \int_S \overset{v}{T_i} \delta u_i \, dS. \tag{4}$$

On substituting $\overset{v}{T_i} = \sigma_{ij} v_{ij}$ in accordance with Lame's stress ellipsoid, we have

$$\int_S \overset{v}{T_i} \delta u_i \, dS = \int_S \sigma_{ij} \delta u_i v_j \, dS = \int_V \left(\sigma_{ij} \delta u_i \right)_{,j} dv$$
$$= \int_V \sigma_{ij,j} \delta u_j \, dv + \int_V \sigma_{ij} \delta u_{i,j} \, dv. \tag{5}$$

According to the equation of equilibrium, the first integral on the right-hand side is equal to $-\int F_i \delta u_i \, dv$. On account of the symmetry of σ_{ij}, the second integral can be written as

$$\int_V \sigma_{ij} \left[\frac{1}{2} \left(\delta u_{i,j} + \delta u_{j,i} \right) \right] dv = \int_V \sigma_{ij} \delta e_{ij} \, dv. \tag{6}$$

Therefore, (6) becomes

$$W = \int_V F_i \delta u_i \, dv + \int_S \overset{v}{T_i} \delta u_i \, dS = \int_V \sigma_{ij} \delta e_{ij} \, dv = \frac{1}{2} \sigma_{ij} e_{ij}. \tag{7}$$

Substituting the generalized Hooke's law into the above equation, Equation (7) can be described by stresses tensor as follows:

$$W = \frac{1}{2E} \left[(1 + \mu) \sigma_{ij} \sigma_{ji} - \mu I \right],$$
$$I = \sum_{i=1}^{3} \sigma_{ij}. \tag{8}$$

As for the surrounding rock near a tunnel or cavity, the stresses state are always presented as tangential stress σ_1, radial stress σ_2, and axial stress σ_3. Then the W is rewritten as

$$U = \frac{1}{2E} \left[\sigma_1^2 + \sigma_2^2 + \sigma_3^2 - 2\nu \left(\sigma_1 \sigma_2 + \sigma_2 \sigma_3 + \sigma_3 \sigma_1 \right) \right]. \tag{9}$$

4.2. Numerical Calculation Model.

Zhazixi Antimony Mine has been mined using shrinkage stoping method over 110 years since 1906, and the mining sequences are chaotic and stress distribution is complex because the rich ore veins are preferential mined. Especially, adjacent veins are too close to interrelate in mining process. At present, no. 1, no. 9, and no. 19 are continuously mined. To analyze stress and energy characteristics of steeply inclined thin veins, five adjacent veins of group I in Zhazixi Antimony Mine are regarded as study objective. According to the mining situation, the numerical model was built from level −25 m to level −205 m

by FLAC^{3D} with the dimension of 300 m (length) × 200 m (width) × 300 m (height) (Figure 12). In the coordinate system of the model, the positive direction of Y-axis and X-axis is northwest 25° and northeast 65°, respectively. The physical and mechanical parameters of rocks are shown in Table 2.

Considering the height of overlying strata is 420 m on top of the model, self-weight stress, calculated by Equation (10), is applied as follows:

$$\sigma_z = \gamma h_z = 27.5 \times 420 = 11.55 \, \text{MPa}, \tag{10}$$

where γ and h_v are the unit weight of the rock mass and the height of the overlying strata, respectively.

Based on Equation (2), the X axis and Y axis of the model are applied maximum principal stress and minimum principal stress, respectively.

According to mining status, four mining sequences have been discussed: (1) mining from hanging wall to footwall, (2) advanced one-level mining, (3) advanced two-level mining, and (4) mining along the inclined direction. Two rows of monitoring lines are arranged on the hanging wall of the 3# vein (Figure 12(b)).

4.3. Strain Energy Evolution during Steeply Inclined Thin Veins Mining.

As demonstrated in Figure 13, a larger pressure relief area with a diameter of 20 m is formed in the footwall of ore vein, which keeps the ore veins of next level to stay in low stress areas by sequence 1. While there is an ellipsoidal pressure relief arch between two adjacent ore veins by sequence 2, it can induce concentrated stress of adjacent veins and make self-weight stress transmit to advanced veins corner along the stress arch, which causes stress increase rapidly. Obviously, the greater the depth of advance mining along the inclined direction of an ore vein, the greater the stress concentration factor at the bottom corner of hanging wall.

Accordingly, the maximum stress concentration factor of sequence 1 near the boundary is only 0.85 based on monitoring results, and the maximum stress concentration factors of sequence 2, sequence 3, and sequence 4 near the boundary are 1.25, 1.37, and 1.52, respectively (Figure 14(a)). Furthermore, the stress concentration occurs in the range of 10 m near bottom corner of the stope, where rockbursts appear easily. At the same time, the transverse influence radius of stress concentration area at the bottom of stope is less than 5 m; that is, the maximum stresses of monitoring line 2 are close to in situ stress (Figure 14(b)).
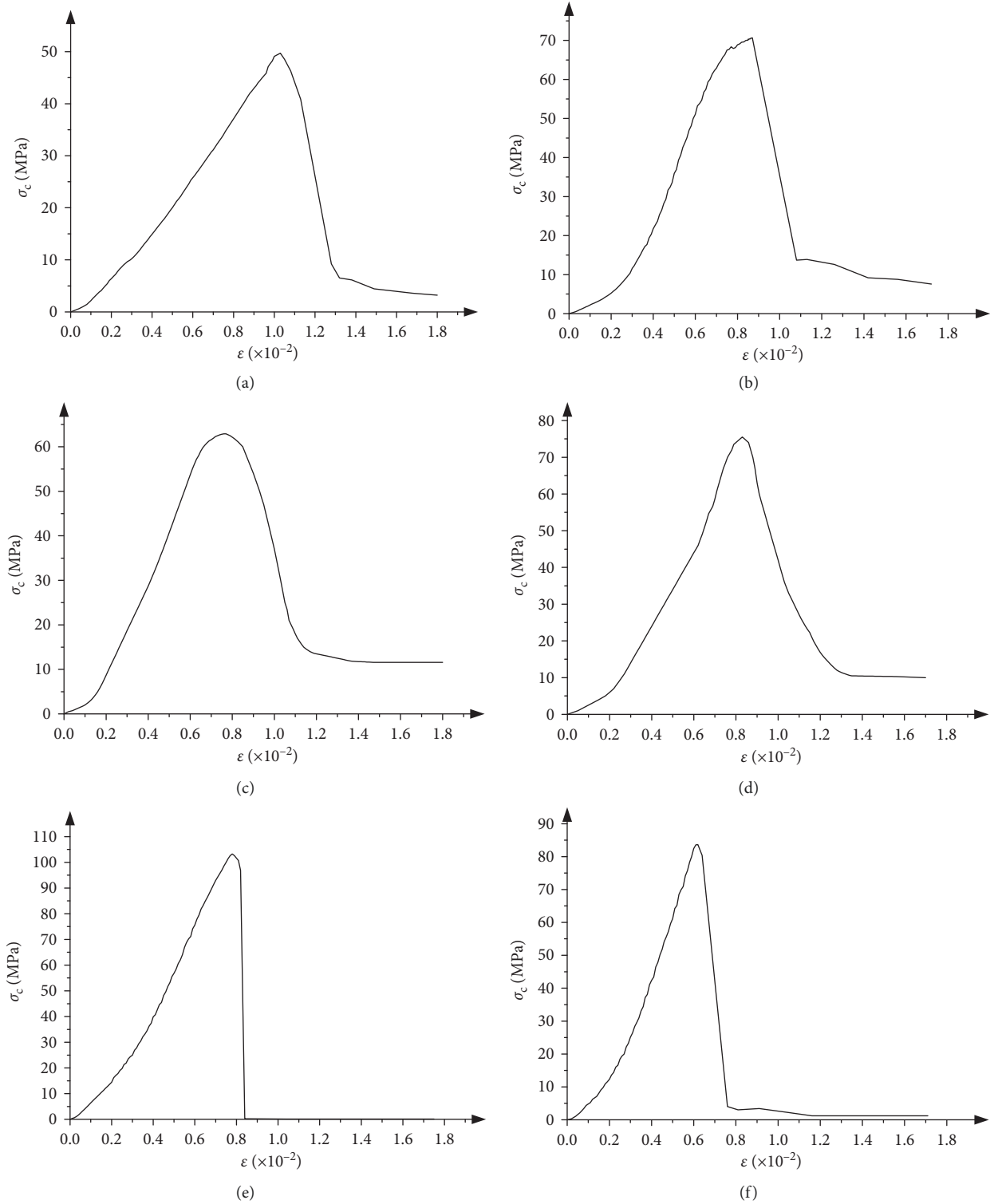
Figure 10: Strain-stress curves of rock masses in Zhazixi Antimony Mine. (a) Slate. (b) Tuffaceous slate. (c) Quartz sandstone. (d) Tuffaceous sandstone. (e) Dense massive stibnite. (f) Disseminated stibnite.

Considering elastic strain energy (Figure 15) and rockburst proneness criteria (Equation (3)) comprehensively, the maximum stress and elastic strain energy often appear in the corner of the hanging wall. Accordingly, the main reasons for different types of rockburst are attributed to mining sequences. To understand the rockburst mechanisms, Figure 15(a) presents the maximum elastic strain energy evolution curves on the corner of each level. By

TABLE 3: Rockburst proneness criteria.

| Criterion	Formula	Empirical value	Correction value	Rockburst intensity
Fissure coefficient (K_v)	$K_v = f(J_v)$	>0.8	>0.75	Strong
		0.6~0.8	0.65~0.75	Moderate
		0.55~0.60	0.55~0.75	Weak
Brittleness coefficient (B)	$B = \sigma_c/\sigma_t$	<14.5	<16.8	Strong
		14.5~26.7	16.8~25	Moderate
		26.7~40	25~40	Weak
Tao discriminant index (α)	$a = \sigma_c/\sigma_1$	≤2.5	≤4	Strong
		2.5~5.5	4~6.3	Moderate
		5.5~14.5	6.3~11.4	Weak
Impact energy index (W_{CF})	$W_{CF} = W_E/W_P$	>3	>3	Strong
		2~3	1.7~2.8	Moderate
		1~2	1~1.7	Weak
Elastic energy index (W_{ET})	$W_{ET} = \sigma_c^2/2E_S$	>200	>300	Strong
		100~200	200~300	Moderate
		50~100	100~200	Weak
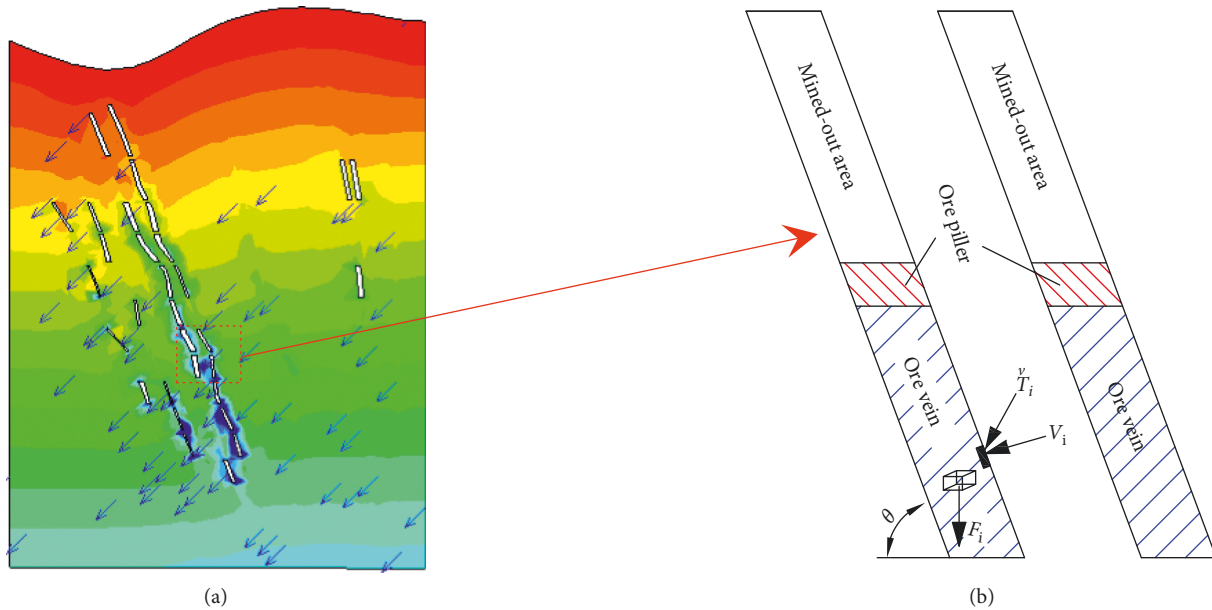
FIGURE 11: The stress state of steeply inclined thin veins. (a) Stress vector. (b) Theoretical stress model.

companion, it has been found that mining sequence 1 will have no rockbursts, and rockbursts may occur at mining sequence 2, mining sequence 3, and mining sequence 4, and the intensity of rockburst increases with mining depth. The deeper the advanced mining level is, the greater the stored elastic strain energy is.

Combined with the process of rock dynamic failure under uniaxial compression test, there may be spalling type of rockburst when the elastic strain energy is less than 200 kJ·m^{-3}; however, when the elastic strain energy exceeds 300 kJ·m^{-3}, throwing-type of rockburst most likely occurs. Especially, the storage elastic strain energy is large enough when mining level surpasses level −115 m, which leads to the strong rockburst accompanied with ejecting or throwing in the mining face firstly. As shown in Figure 15(b), the elastic strain energy stored in rock masses far away from mining face 5 m are less than 200 kJ·m^{-3}, and they might produce spalling type of rockburst. Based on the superposition effect of elastic strain energy, it produces a large scale of strong rockburst.

5. Rockburst Validation

Based on statistics data, there were 30 rockburst events between May 2012 and May 2013 in Zhazixi Antimony Mine. During this period, a prospecting tunnel ore vein was excavated at −115 m level, three stopes ore vein was mined at −160 m level, a main haulage roadway was excavated, and two stopes were cut at −205 m level. The evolution mechanism of rockburst can be summarized as follows.

Rockburst began to appear when mining depth reached −115 m level where the elastic strain energy exceeded
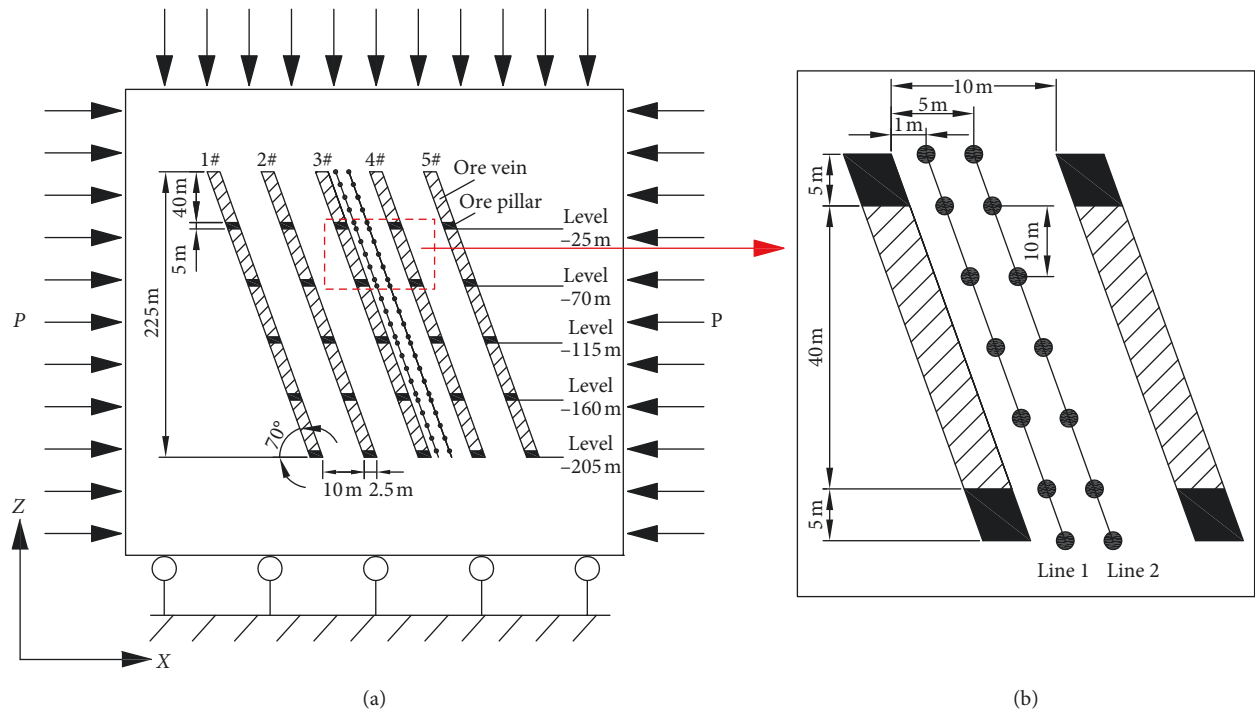
(a)

(b)

FIGURE 12: (a) Numerical calculation model and (b) monitoring points layout.
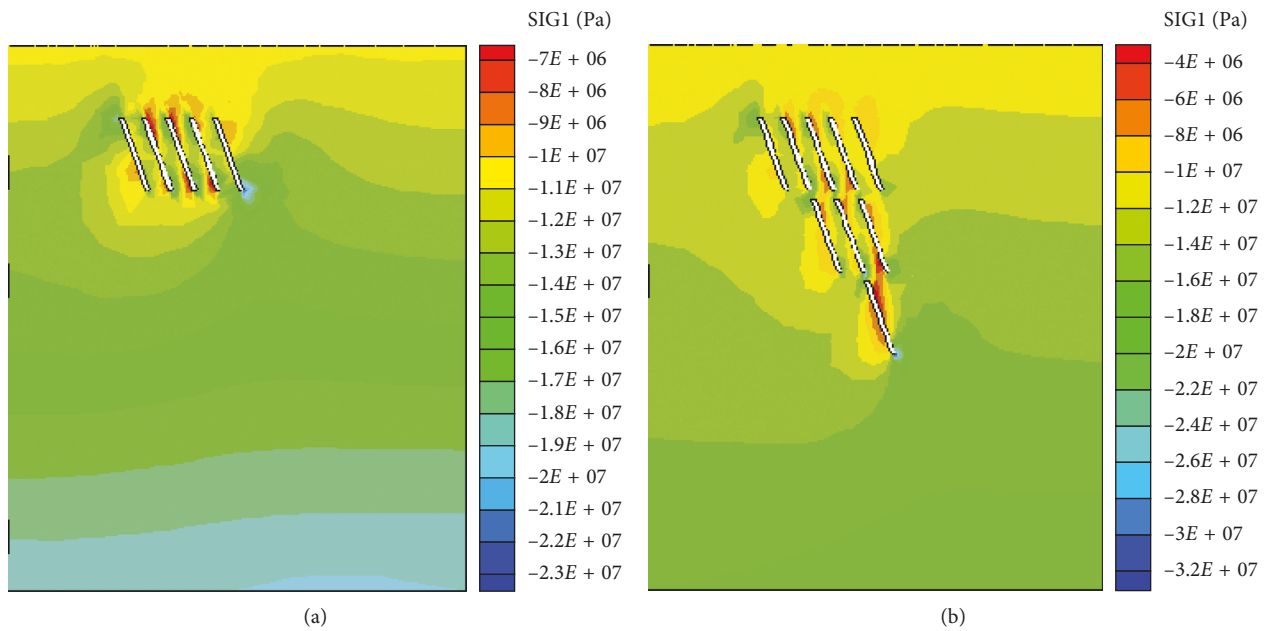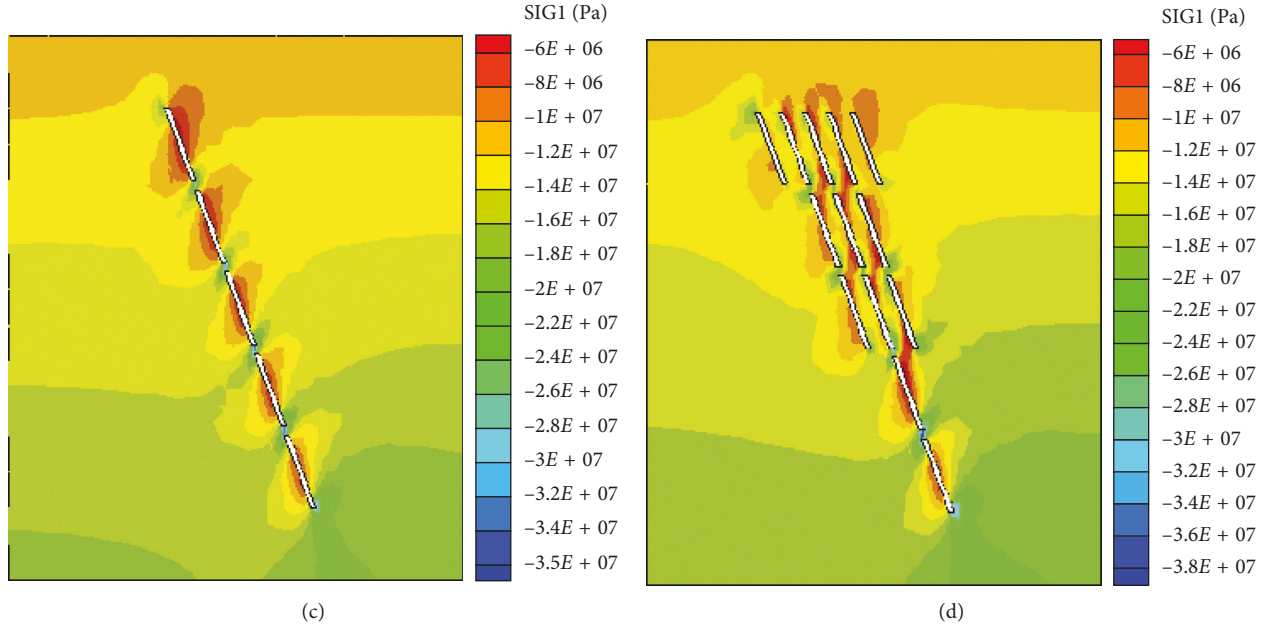

(a)

(b)

FIGURE 13: Continued.

FIGURE 13: The principal stress nephogram. (a) Sequence 1. (b) Sequence 2. (c) Sequence 3. (d) Sequence 4.
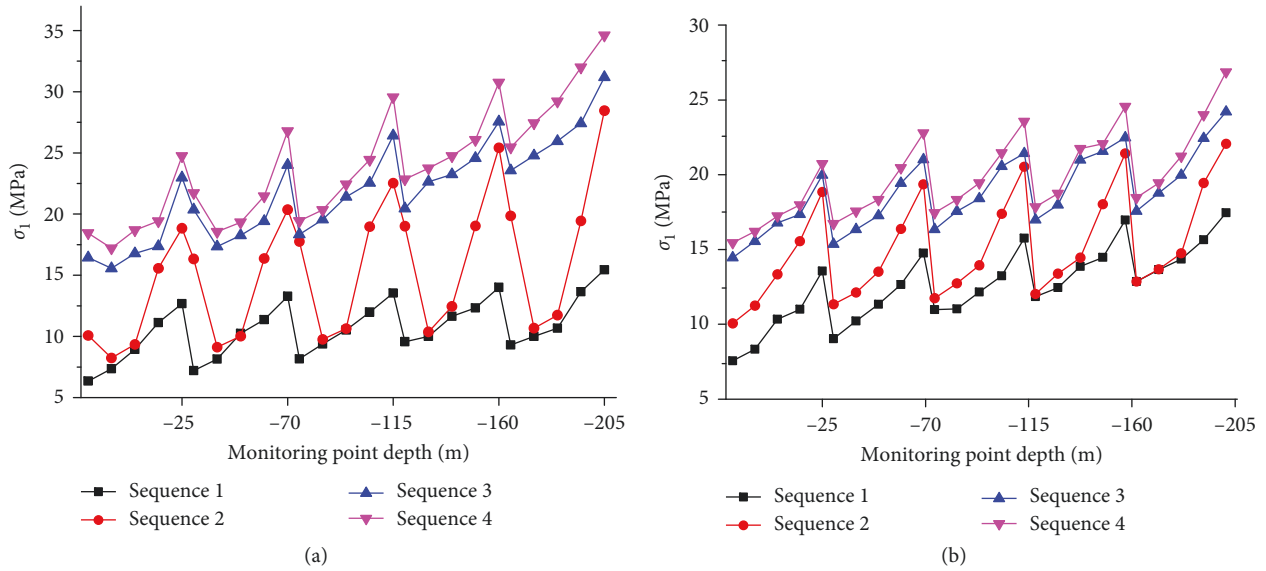

FIGURE 14: The maximum principal stress values evolution with depth. (a) Monitoring line 1. (b) Monitoring line 2.

$100 \, \text{kJ} \cdot \text{m}^{-3}$ according to the numerical results. When mining to $-160 \, \text{m}$, mining activities caused local stress concentration where elastic strain energy exceeds $350 \, \text{kJ} \cdot \text{m}^{-3}$, resulting in frequent occurrence of different types of rockburst, as shown in Figure 16(a).

Rockburst intensity is closely related to rock mechanical properties (Figure 16(b)). Especially, slate is prone to spalling rockburst with poor capacity of stored elastic strain energy because of the smooth internal structural plane, but massive stibnite could withstand great pressure and accumulate great elastic strain energy due to good integrity; hence, they generally occur strong rockburst in the high stress area.

According to the characteristics of shallow-hole shrinkage stoping, stopes and ventilation shafts are generally arranged along the ore veins, so they often appear high-intensity rockbursts because of the special physical and mechanical properties of stibnite.

Above all, it is effective to predict rockburst combined with rockburst proneness criteria and numerical stimulation analysis in Zhazixi Antimony Mine.

6. Conclusions

(1) Stress relief method by overcoring is utilized to obtain in situ stress of four measurement points in Zhazixi
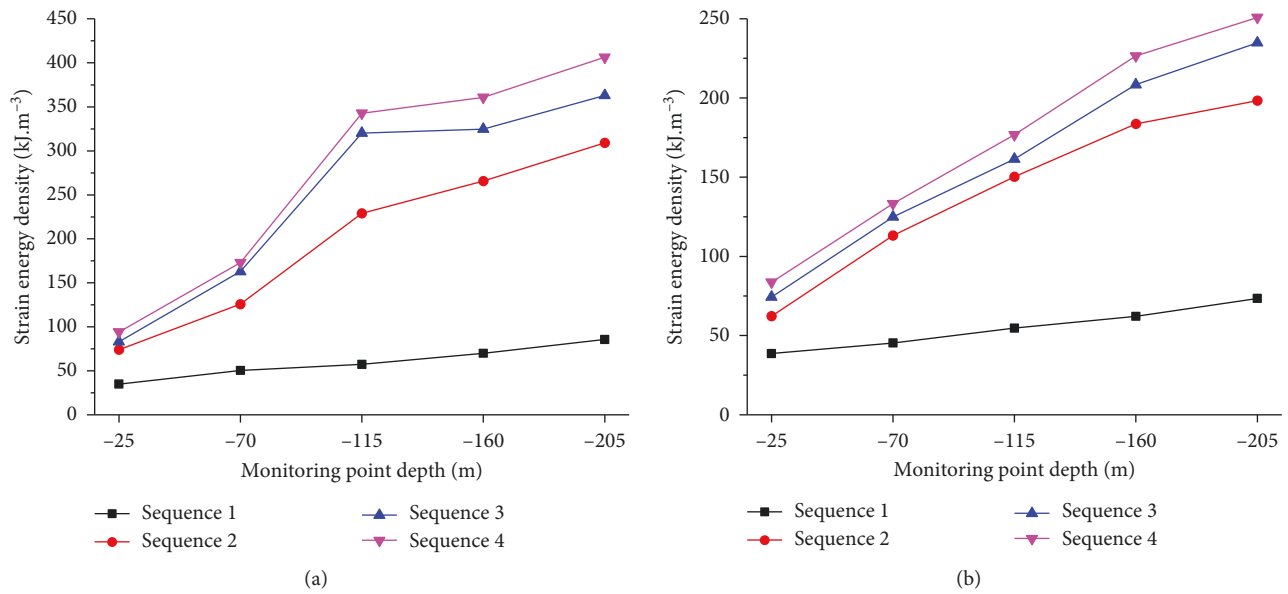
(a)

(b)

Figure 15: The maximum elastic strain energy evolution with depth. (a) Monitoring line 1. (b) Monitoring line 2.
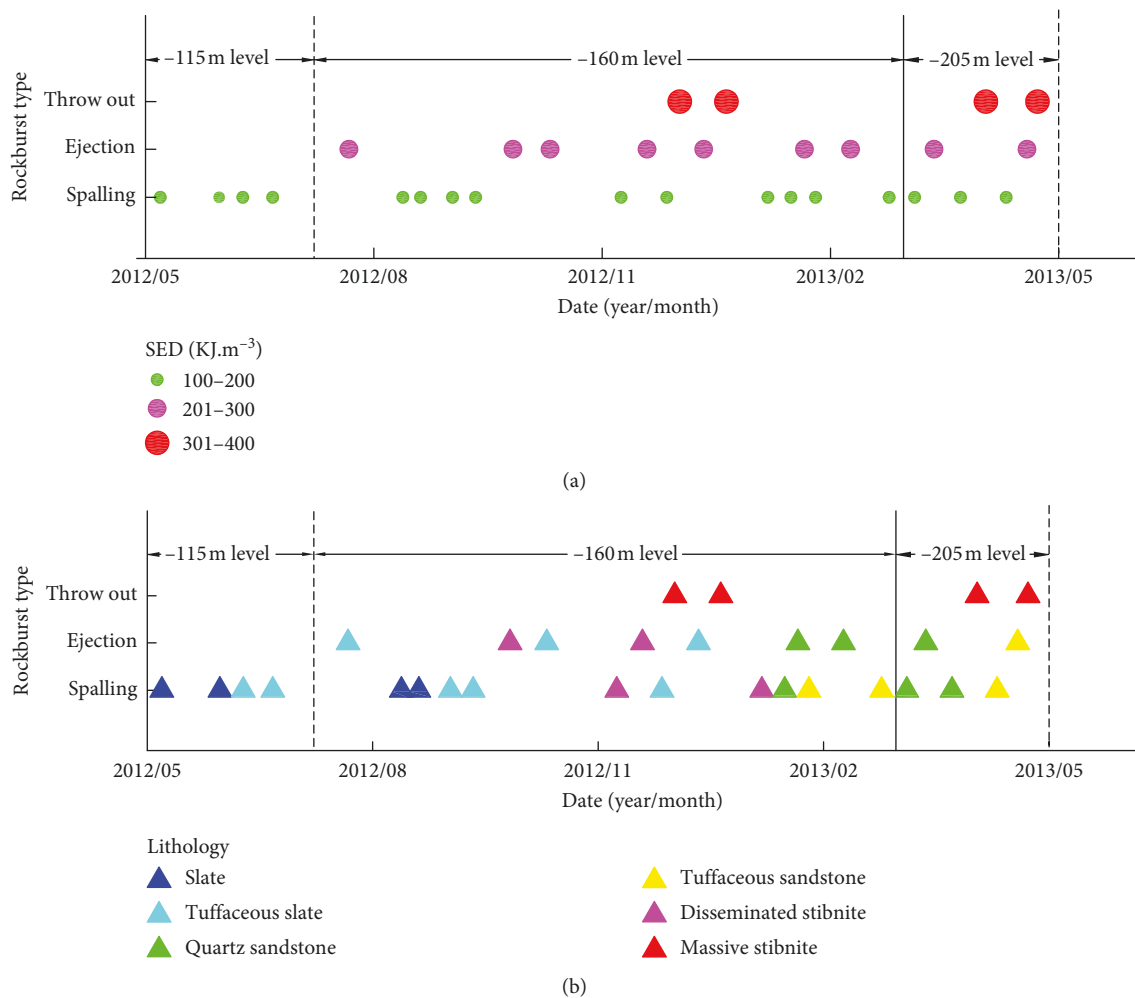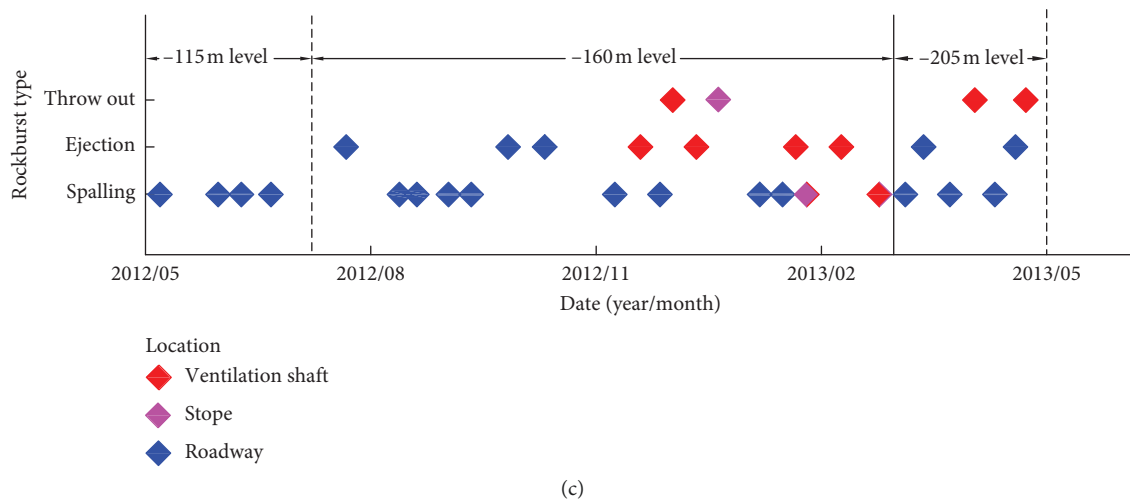

(a)

(b)

Figure 16: Continued.

(c)

FIGURE 16: Verification of rockburst events between May 2012 and May 2013. (a) Rockburst type and strain elastic energy. (b) Rockburst type and lithology. (c) Rockburst type and location.

antimony. The in situ measurement results show that the major principal stress exceeds 20 MPa with the NEE-SWW direction in deep mining areas. Furthermore, the principal stress distribution regulations in Zhazixi Antimony Mine are summed up.

(2) With respect to the influence of lithology, uniaxial compression tests are carried out towards six kinds of rocks. Combined with field geological survey and in situ measurements in Zhazixi Antimony Mine, five criteria of rockburst proneness are corrected to qualitative analyzed rockburst conditions. Consequently, rockburst proneness criteria of Zhazixi Antimony Mine are put forward.

(3) According to the distribution characteristics of steeply inclined thin veins, the stress and elastic strain energy evolution are analyzed by numerical simulation in four mining sequences. The results reveal advanced mining is the main factor to energy accumulation. The deeper the advanced mining is, the greater the stored elastic strain energy is. Enough elastic strain energy can also induce deep elastic strain energy release to cause chain reaction of large-scale rockbursts.

(4) Comparing rockburst events with prediction results, the unanimous conclusions have been drawn: throwing-type rockbursts frequently occur in massive stibnite of ventilation shaft and stope where the elastic strain energy exceeds $300 \, \text{kJ} \cdot \text{m}^{-3}$ due to the influence of mining sequence, spalling-type rockbursts generally appear in slate of roadway where the elastic strain energy exceeds $100 \, \text{kJ} \cdot \text{m}^{-3}$ under high stress state, and ejection-type rockbursts arise in different rock masses under a certain condition.

Data Availability

The data used to support the findings of this study are included within the article.

Conflicts of Interest

The authors declare that there are no conflicts of interest regarding the publication of this paper.

References

[1] T. B. Li, C. C. Ma, M. L. Zhu, L. B. Meng, and G. Q. Chen, "Geomechanical types and mechanical analyses of rockbursts," *Engineering Geology*, vol. 222, no. 3, pp. 72–83, 2017.

[2] X. T. Feng, Y. Yu, G. L. Feng, Y.-X. Xiao, B.-R. Chen, and Q. Jiang, "Fractal behaviour of the microseismic energy associated with immediate rockbursts in deep, hard rock tunnels," *Tunnelling and Underground Space Technology*, vol. 51, no. 1, pp. 98–107, 2016.

[3] J. M. Wang, X. H. Zeng, and J. F. Zhou, "Practices on rockburst prevention and control in headrace tunnels of Jinping II hydropower station," *Journal of Rock Mechanics and Geotechnical Engineering*, vol. 4, no. 3, pp. 258–268, 2012.

[4] J. P. Yang, W. Z. Chen, W. S. Zhao et al., "Geohazards of tunnel excavation in interbedded layers under high in situ stress," *Engineering Geology*, vol. 230, no. 9, pp. 11–22, 2017.

[5] X. X. Liu, S. B. Zhan, Y. B. Zhang, X. Wang, Z. Liang, and B. Tian, "The mechanical and fracturing of rockburst in tunnel and its acoustic emission characteristics," *Shock and Vibration*, vol. 2018, Article ID 3503940, 11 pages, 2018.

[6] M. F. Cai, "Prediction and prevention of rockburst in metal mines-a case study of Sanshandao gold mine," *Journal of Rock Mechanics and Geotechnical Engineering*, vol. 8, no. 2, pp. 204–211, 2016.

[7] X. Y. Feng, J. P. Liu, B. R. Chen, Y. Xiao, G. Feng, and F. Zhang, "Monitoring, warning, and control of rockburst in deep metal mines," *Engineering*, vol. 3, no. 4, pp. 538–545, 2017.

[8] W. Lei, L. Q. Huang, A. Taheri, and X. Li, "Rockburst characteristics and numerical simulation based on a strain energy density index: a case study of a roadway in Linglong gold mine, China," *Tunnelling and Underground Space Technology*, vol. 69, pp. 223–232, 2017.

[9] S. Afraei, K. Shahriar, and S. H. Madani, "Statistical assessment of rock burst potential and contributions of considered

predictor variables in the task," *Tunnelling and Underground Space Technology*, vol. 72, pp. 250–271, 2018.

[10] S. J. Li, X. T. Feng, Z. H. Li, B. Chen, C. Zhang, and H. Zhou, "In situ monitoring of rockburst nucleation and evolution in the deeply buried tunnels of Jinping II hydropower station," *Engineering Geology*, vol. 137-138, no. 7, pp. 85–96, 2012.

[11] S. J. Miao, M. F. Cai, Q. F. Guo, and Z. J. Huang, "Rock burst prediction based on in-situ stress and energy accumulation theory," *International Journal of Rock Mechanics and Mining Sciences*, vol. 83, no. 2, pp. 86–94, 2016.

[12] G. S. Su, Y. J. Shi, X. T. Feng, J. Jiang, J. Zhang, and Q. Jiang, "True-triaxial experimental study of the evolutionary features of the acoustic emissions and sounds of rockburst process," *Rock Mechanics and Rock Engineering*, vol. 51, no. 2, pp. 375–389, 2018.

[13] F. Z. Meng, H. Zhou, Z. Q. Wang et al., "Experimental study on the prediction of rockburst hazards induced by dynamic structural plane shearing in deeply buried hard rock tunnels," *International Journal of Rock Mechanics and Mining Sciences*, vol. 86, no. 2, pp. 210–223, 2016.

[14] Q. J. Zhu, Y. Feng, M. Cai, J. H. Liu, and H. H. Wang, "Interpretation of the extent of hydraulic fracturing for rockburst prevention using microseismic monitoring data," *Journal of Natural Gas Science and Engineering*, vol. 38, no. 6, pp. 107–119, 2017.

[15] Q. Y. Zhang, X. T. Zhang, Z. C. Wang, W. Xiang, and J. Xue, "Failure mechanism and numerical simulation of zonal disintegration around a deep tunnel under high stress," *International Journal of Rock Mechanics and Mining Sciences*, vol. 93, pp. 344–355, 2017.

[16] W. C. Zhu, Z. H. Li, L. Zhu, and C. A. Tang, "Numerical simulation on rockburst of underground opening triggered by dynamic disturbance," *Tunnelling and Underground Space Technology*, vol. 25, no. 5, pp. 587–599, 2010.

[17] L. S. Jiang, P. Wang, P. P. Zhang, P. Q. Zheng, and B. Xu, "Numerical analysis of the effects induced by normal faults and dip angles on rock bursts," *Comptes Rendus Mécanique*, vol. 345, no. 10, pp. 690–705, 2017.

[18] L. Driad-Lebeau, F. Lahaie, M. Al Heib, J. P. Josien, P. Bigarré, and J. F. Noirel, "Seismic and geotechnical investigations following a rockburst in a complex French mining district," *International Journal of Coal Geology*, vol. 64, no. 1-2, pp. 66–78, 2005.

[19] X. P. Zhou, Q. H. Qian, and H. Q. Yang, "Rock burst of deep circular tunnels surrounded by weakened rock mass with cracks," *Theoretical and Applied Fracture Mechanics*, vol. 56, no. 2, pp. 79–88, 2011.

[20] K. Holub and V. Petros, "Some parameters of rockbursts derived from underground seismological measurements," *Tectonophysics*, vol. 456, no. 1-2, pp. 67–73, 2008.

[21] C. P. Lu, Y. Liu, N. Zhang, T.-B. Zhao, and H.-Y. Wang, "In-situ and experimental investigation of rockburst precursor and prevention induced by fault slip," *International Journal of Rock Mechanics and Mining Sciences*, vol. 108, pp. 86–95, 2018.

[22] F. Z. Meng, H. Zhou, Z. Q. Wang et al., "Experimental study of factors affecting fault slip rockbursts in deeply buried hard rock tunnels," *Bulletin of Engineering geology and the environment*, vol. 76, no. 3, pp. 1167–1182, 2017.

[23] S. Zhong, Q. Jiang, X. T. Feng et al., "A case of in-situ stress measurement in Chinese Jingping underground laboratory," *Rock and Soil Mechanics*, vol. 39, no. 1, pp. 356–366, 2018.

[24] G. Y. Zhu, X. H. Guo, W. Z. Chen et al., "Inversion of in-situ stress and its application in Xuefengshan roadway tunnel," *Central South Highway Engineering*, vol. 31, no. 1, pp. 71–75, 2006, in Chinese.

[25] S. W. Duan and X. E. Xu, "Discussion of problems in calculation and application of rock mass integrity coefficient," *Journal of Engineering Geology*, vol. 21, no. 4, pp. 548–552, 2013, in Chinese.

[26] J. A. Wang and H. D. Park, "Comprehensive prediction of rockburst based on analysis strain energy in rocks," *Tunnelling and Underground Space Technology*, vol. 16, no. 1, pp. 49–57, 2001.

[27] Y. C. Fung, *Foundations of Solid Mechanics*, Prentice-Hall, Upper Saddle River, NJ, USA, 1977.

Journal of
Engineering

The Scientific
World Journal

International Journal of
Rotating
Machinery

Journal of
Sensors

Advances in
Multimedia

Advances in
Civil Engineering

Journal of
Control Science
and Engineering

Journal of
Robotics

Journal of
Electrical and Computer
Engineering

Advances in
OptoElectronics

VLSI Design

International Journal of
Navigation and
Observation

Modelling &
Simulation
in Engineering

International Journal of
Aerospace
Engineering

International Journal of
Chemical Engineering

International Journal of
Antennas and
Propagation

Active and Passive
Electronic Components

Shock and Vibration

Advances in
Acoustics and Vibration